

Particle Image Velocimetry Measurement of Unsteady Turbulent Flow around Regularly Arranged High-Rise Building Models

Sato, Tsuyoshi

Interdisciplinary Graduate School of Engineering Sciences, Kyushu University

Hagishima, Aya

Interdisciplinary Graduate School of Engineering Sciences, Kyushu University

Ikegaya, Naoki

Interdisciplinary Graduate School of Engineering Sciences, Kyushu University : Assistant Professor

Tanimoto, Jun

Interdisciplinary Graduate School of Engineering Sciences, Kyushu University : Professor

<https://hdl.handle.net/2324/1434330>

出版情報 : International Journal of High-Rise Buildings. 2 (2), pp.105-113, 2013-06. Korean Council on Tall Building and Urban Habitat

バージョン :

権利関係 :

Particle Image Velocimetry Measurement of Unsteady Turbulent Flow around Regularly Arranged High-Rise Building Models

T. Sato[†], A. Hagishima, N. Ikegaya, and J. Tanimoto

Interdisciplinary Graduate School of Engineering Sciences, Kyushu University, Fukuoka 816-8580, Japan

Abstract

Recent studies proved turbulent flow properties in high-rise building models differ from those in low-rise building models by comparing turbulent statistics. Although it is important to understand the flow characteristics within and above high-rise building models in the study of urban environment, it is still unknown and under investigation. For this reason, we performed wind tunnel experiment using Particle Image Velocimetry (PIV) to investigate and identify the turbulent flow properties and characteristic flow patterns in high-rise building models. In particular, we focus on instantaneous flow field near the canopy and extracted flow field when homogeneous flow field were observed. As a result, six characteristic flow patterns were identified and the relationship between these flow patterns and turbulent organized structure were shown.

Keywords: Particle image velocimetry, High rise building model, Turbulent statistics, Unsteady flow field, Turbulent organized structure

1. Introduction

The accurate estimation of wind characteristics within and above an urban canopy layer has been one of important issues in terms of the dispersion of pollutants, the thermal comfort of pedestrians and heat transfer between urban surfaces and the atmosphere. Thus, numerous studies based on wind tunnel experiments, computational simulations, and field observations have been performed for more than decades.

One of important aerodynamic features of an urban canopy layer is three contrasting regimes of mean flow field observed around buildings according to the condition of building spacing, namely isolated flow, wake interference flow, and skimming flow, (e.g., Oke, 1988). Such transition of mean flow pattern is caused by the interference of eddies around each building, and it is consistent with the fact that roughness length, which is a length scale of momentum absorption by buildings used in a logarithmic similarity theory, exhibits a single peak against urban roughness density (e.g., Grimmond and Oke, 1999). Therefore, various studies on the relation between aerodynamic parameters and urban geometry have been performed.

In addition to researches on bulk aerodynamic characteristics of urban roughness, three dimensional flow fields within urban canopy layers of several types of block arrays have been also intensively investigated. For example, Coceal et al. (2006) performed Direct Numerical Si-

mulation (DNS) of flow over cubical arrays with plan area index (λ_p) 25 %, and visualized instantaneous coherent structures of turbulence around cubes. In addition, they revealed the different features of mean flow pattern and turbulent statistics between a staggered array and square array. Kanda (2006) conducted Large Eddy Simulation (LES) on flow over cubical arrays with square and staggered layouts under various λ_p conditions and presented the results of quadrant analysis and snapshots indicating turbulent organized structure (TOS). Michioka et al. (2011) investigated the effect of TOS on pollutant removal from a two dimensional canyon with a building-height to street width ratio of 1 based on LES.

Since the pioneering work done by Adrian et al. (2000) on TOS over a smooth wall boundary, which consists of hairpin packets and low-momentum streaks, experimental studies on instantaneous flow field over various rough walls have been recently reported along with the development of the various measurement techniques such as particle image velocimetry (PIV). Huq et al. (2007) conducted a PIV experiment of flow over two types of uniform block arrays of λ_p 18.6% with different conditions of average building height-to width ratio 1 and 3 using a water tunnel, and presented that streamwise velocity profiles differ due to building height-to width ratio. Pokrajac et al. (2007) conducted a PIV measurement of flow over a 2-D bar roughness and investigated the characteristics of dispersive stress and spatial distribution of mean flow. Takimoto et al. (2011) performed an outdoor and indoor experiment of flow within and above a cube array by using PIV technique and they found out a characteristic flow structure termed as 'flushing' for instantaneous velo-

[†]Corresponding author: T. Sato
Tel: +81-(0)80-1740-9180
E-mail: 2es12133w@s.kyushu-u.ac.jp

city field and investigated the correlation between the flushing events and large scale TOS over the block array. Reynolds and Castro (2008) measured flow field within and above a staggered cubical array based on PIV and laser-Doppler velocimetry (LDV), and investigated the features of turbulent statistics.

Most of these studies focus on the flow field over arrays consist of cubes or short blocks characterized by low aspect ratio (ratio of frontal area to roof area). Although such geometry conditions might be suitable for simplifying residential districts of detached houses or traditional European cities, airflow characteristics of real urban areas consist of not only low-rise buildings but also slender high-rise buildings are difficult to be modeled. In particular, several researchers pointed out that various other geometry factors such as height variability, rotation angle of blocks against mean flow direction, and slenderness of blocks, affect the flow field and the drag force based on their experimental results. According to the effect of slenderness of blocks, Hagishima et al. (2012) measured drag coefficients (C_d) of staggered uniform block arrays with various conditions, and presented that the relations between C_d and λ_p are different by the block slenderness and block rotation angle. This result suggests that 1) aspect ratio is an index of both slenderness and streamline nature of a roughness element, 2) the flow field around a slender block array with high aspect ratio is different from the typical skimming flow observed around block arrays with low-aspect ratio under high λ_p condition due to the less bluff-body nature. In fact, Li et al. (2008) conducted numerical simulation of flow over a block array with high aspect ratio using LES and investigated vertically aligned primary recirculation of mean flow within the canopy.

Although these researches imply the necessity of considering the flow around high-rise building arrays, the existing data is still limited, and the holistic features have not been clarified. Under these circumstances, in this study, we observed flow field within and above a building-model array comprises slender rectangular blocks by using PIV method in a wind tunnel. The experimental set-up is outlined in the following section and the profiles of turbulent statistics as well as the result of quadrant analysis are presented in Sect. 3. Subsequently, in Sect. 4, we depict several typical features of instantaneous flow field, and Sect. 5 presents discussion and major conclusion.

2. Experimental Set-up

2.1. Wind tunnel and configuration of the array

The experiment was conducted in the wind tunnel at the Interdisciplinary Graduate School of Engineering Sciences, Kyushu-university, Japan. The facility was a low-speed single-return tunnel with a test section of height 1 m, width 1.5 m and length 19.5 m including an underground pit. The floor of the test section with a length of 8 m was

covered by a block array. All blocks made from wood with a uniform base of 8 mm × 8 mm and height of 25 mm were arranged in the staggered layout with plan area ratio $\lambda_p = 4\%$. The layout of the measurement system and block array is schematically shown in Figures 1 and 2.

2.2. Particle image velocimetry set-up

The PIV measurement was performed by illuminating oil particles of about 1 mm diameter with a 3 mm thick light sheet produced by Nd:YAG 2W laser (operating at 532 nm) and plano-concave lens (focus length is -20 mm). The images were photographed at a frequency of 1000 Hz for a period of 43.6 seconds by using a CCD camera (FASTCOM SA-X, Photron, 512×512 pixel) with a lens of 85 mm length f/2.8 (PC Micro-Nikkor 85mm f/2.8D, Nikon). The laser sheet was introduced from the laser generator placed beneath the wind tunnel floor through an acrylic plate to the measurement target area (56 mm × 70 mm) in a streamwise and wall normal plane. The position of the laser sheet was shown in Fig. 2 and the camera was placed out of the wind tunnel at a distance of 470 mm from the light sheet in spanwise direction.

Local displacement of a particle image was determined by a correlation coefficient of particle brightness pattern calculated at a frequency of 500 Hz by the FFT-based cross-correlation method developed by Willert and Gharid (1990), and it is transformed into the instantaneous wind velocity. The correlation coefficient is calculated by the following process: an integration area is selected on a PIV photograph and another integration area is defined at the same location of contiguous PIV photograph, and then a correlation coefficient of the particle brightness pattern

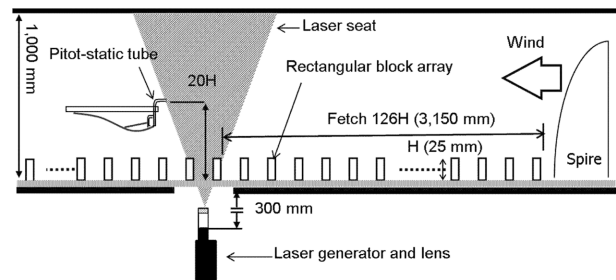


Figure 1. Side view of experimental set up.

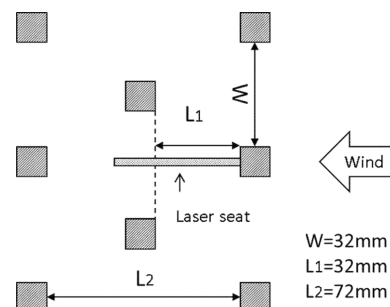


Figure 2. Schematic plan view of block array and the position of laser seat.

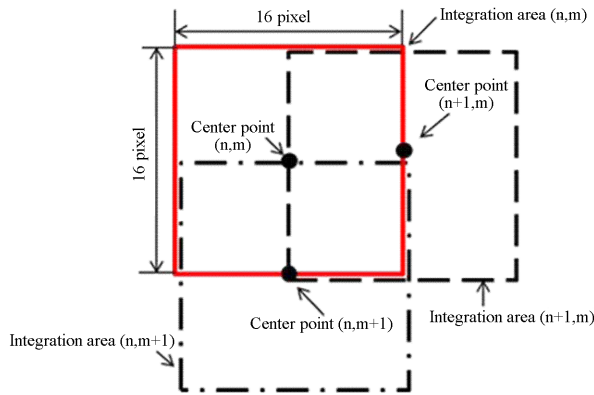


Figure 3. Size and position definition of integration area.

is calculated. A sub-pixel scale analysis is subsequently performed to determine the displacement of particles in smaller scale. Each adjacent integration area overlapped by 50% region, in other words, the center of an integration area is located on the side of the next integration area as shown in Fig. 3, thus wind vectors are obtained each 8 pixel.

After all wind vectors are obtained, data validation is performed for a post processing to remove erroneous wind vectors using two types of linear filters: dynamic mean filter and median filter. Dynamic mean filter is used to identify the erroneous wind vector which has abnormally large absolute value compared to vectors surrounding the target vector, and median filter is employed to determine and remove erroneous vector which is not consistent with the general tendency of surrounding vectors (Westerweel, 1994).

After erroneous vectors are removed, the alternative vectors are calculated based on the second largest peaks of correlation coefficients in each integration areas and validated by the same method. If these vectors are confirmed to be invalid or an adequate secondary peak of correlation coefficient does not exist, interpolated vectors are calculated based on surrounding vectors. Since ratio of the number of interpolated vectors to that of valid vectors was only 3.44%, thus the influence of interpolation seemed to be not so large.

Prior to the main analysis, we validated our experimental data based on the spatial distribution of turbulent statistics and time series fluctuation of streamwise and vertical wind component, and determined the target area for the analysis in which noise effect is relatively small and experimental data seems accurate (Fig. 4).

3. Experimental Result

3.1. Streamwise velocity

Several studies suggest that turbulent flow properties around block arrays with high aspect ratio are similar to those appear in vegetation canopy, for example, Huq et al. (2007) performed a water tunnel experiment using two

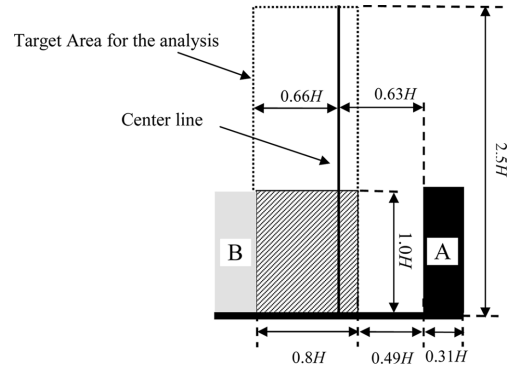


Figure 4. Dotted square: Experimental data has high accuracy, Solid line: center of measurement area.

types of blocks with aspect ratio 1.0 and 3.3 as simplified models of the midtowns of Los Angeles and New York City. They indicated the similarity of vertical profiles of streamwise velocity between vegetation canopy and urban-like canopy consists of high aspect ratio blocks. Furthermore, Moriwaki et al. (2009) conducted a series of field measurement in a rice paddy field and two types of block arrays with aspect ratio 1.0 and 3.3 ($\lambda_p = 0.25$) under almost stable condition and showed the difference and similarity of turbulent statistics and momentum transfer among these three canopies. In this section, we compare the several turbulent statistics obtained in present experiment with a variety of the previous data for vegetation canopy.

Fig. 5(a) shows vertical profiles of U/U_H (U_H is the time-averaged streamwise wind velocity at the canopy height) measured at the center of the measurement area (dotted line shown in Fig. 4). The turbulent statistics presented in Raupach et al. (1996), which are based on field observations and wind tunnel experiments for various types of vegetation canopy and plant like models, are also included in the graphs. The mean wind profile of this experiment shows good agreement with those for vegetation canopy. U/U_H between a height from $0.3H$ to $0.7H$ obtained by our experiment is in a range from 0.46 to 0.50 and almost constant with height; this tendency coincides in particular with that of Uriarra forest (Denmead and Bradley, 1987). In addition to that, the mean wind profiles of both the present experiment and Uriarra forest exhibit two inflection points within the canopy. Similar inflection points within the canopy are also founded in the data of LES simulation (Kanda et al. (2004), a square array of cubical obstacles, $\lambda_p = 0.25$) and field experiment (Baldocchi and Meyers, 1988), a forest consists of mixing species stand of predominantly oak and hickory trees, the average height is 23 m and frontal area index (ratio of projected area to roof area $\lambda_f = 2.5$).

On the other hand, although wind profile of this study are in correspondence with those of Amiro Spruce (Amiro, 1990) and Baldocchi decid (Baldocchi and Meyers, 1988), the difference of wind profiles among each experiment become large above canopy height, and wind profile of

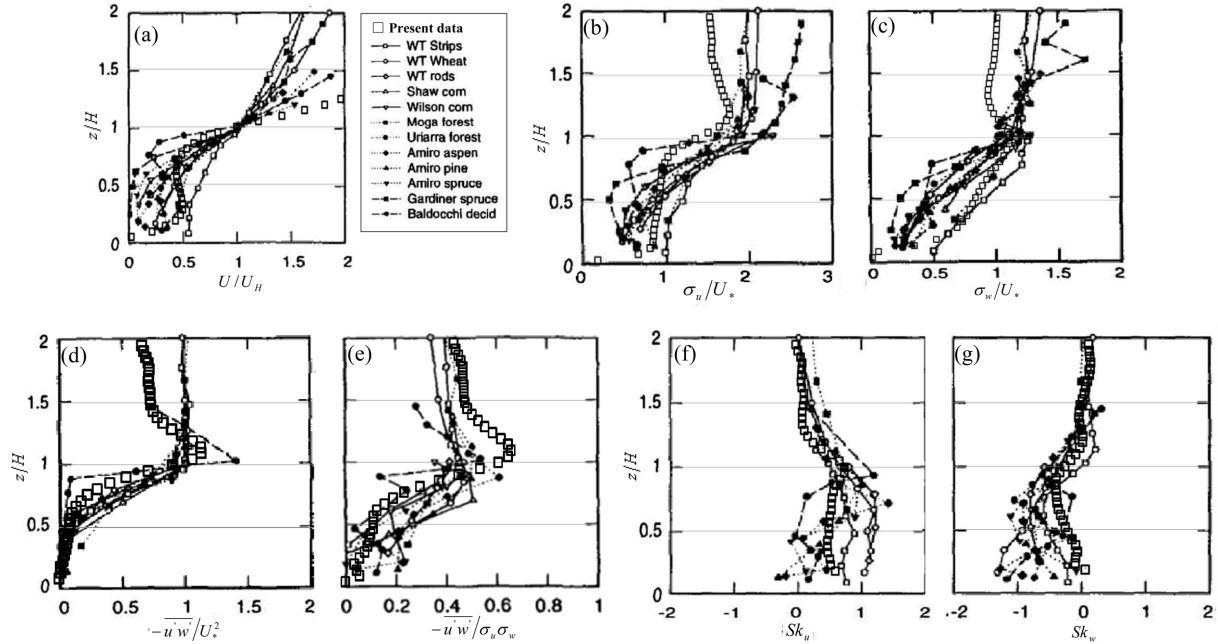


Figure 5(a)-(g). Comparison of vertical profiles of streamwise wind velocity and turbulent statistics in various types of vegetation canopies and present study. All profiles of present experiment are measured at the center of the measurement area (Fig. 4). U_{1H} is time averaged streamwise velocity measured at canopy roof height on the line. (a) U/U_H , (b) σ_u/U_* , (c) σ_w/U_* , (d) Sk_u , (e) Sk_w , (f) $-\overline{u'w'}/U_*^2$, (g) $-\overline{u'w'}/\sigma_u\sigma_w$.

our experiment shows relatively large value compared to those in vegetation canopies. Raupach et al. (1996) suggested such difference is attributed to the difference of canopy morphology characterized by leaf area density (LAD). Although the block array used in this study consists of slender blocks with relatively high aspect ratio compared to ordinary cube arrays and the shape of them is relatively similar to those of tree trunk, the morphology differs from those of vegetation near the canopy top, hence it is thought that difference of wind profiles appeared only above the canopy top.

3.2. Turbulent statistics

Fig. 5(b) and (c) show standard deviation of streamwise and vertical wind velocity normalized by friction velocity (U_*) which is defined by a peak value of spatial averaged Reynolds stress ($z/H = 1.14$) with the data from Raupach et al. (1996). The profiles for two components obtained in the present experiment within the canopy ranges in the scatter of the data of vegetation canopy, in contrast, they are little smaller than those of vegetation canopies above canopy height.

Same tendency is observed in Fig. 5(d) and (e), which show vertical profile of Reynolds stress and uw correlation coefficient ($\overline{u'w'}/(\sigma_u\sigma_w)$). The value of the Reynolds stress in this research is little smaller above canopy but well accorded with the others in plant canopies under a height of $z = 1H$. On the other hand, the values of uw correlation coefficient are relatively similar except for the layer from $1H$ to $1.4H$ and almost constant above z/H

$= 1.4$. Normalized constant value of uw correlation coefficient above canopy height is observed in previous study (e.g., Macdonald et al., 2002). Raupach et al. (1996) defined flow properties in surface, mixing and canopy layer by investigating turbulent statistics and suggested that the typical value of uw correlation coefficient in mixing layer is -0.44 , meanwhile, the value of uw correlation coefficient in present study above $z/H = 1.4$ fluctuates between 0.430 to 0.485 (Fig. 5(e) shows inverse signed uw correlation coefficient). This fact indicates the similarity of flow properties between vegetation canopy and urban like models with high-rise building models.

By contrast, skewness of both two wind components presented in Fig. 5(f) and (g) correspond well with the profile of them in vegetation canopies for both within and above the canopy. It is noteworthy that skewness of streamwise velocity is positive within the canopy and that of vertical component is negative between a height from $0.5H$ to $1.1H$. This tendency is associated with the transition of a mechanism of momentum transfer which is strongly related to intermittent flow patterns in canopy layer as described below.

Quadrant technique was applied for the data of the target area shown in Fig. 4, and the contribution of each quadrant for momentum transfer was calculated by a following equation.

$$\langle \overline{S}_j \rangle = \left\langle \frac{\sum_i^N (u_i' w_i')}{N \times U_*^2} \right\rangle \quad (j=1,2,3,4) \quad (1)$$

Here, $\langle \rangle$ represents a horizontal average in the target area

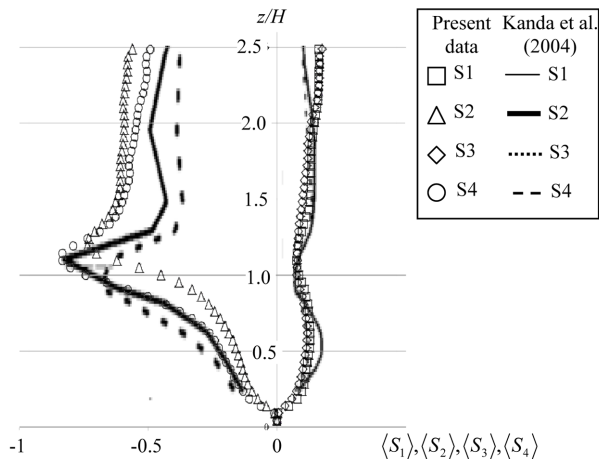


Fig. 6. Special averaged profile of contribution for the momentum transfer by four quadrants. Square, triangle, diamond and circle plots are from this study; thin, solid, dotted and broken line are from Kanda(2004).

and N means the number of time-series data (=21840).

Figure 6 shows the vertical profile of the contribution of each flow mode for momentum transfer and the results of Kanda et al. (2004) based on LES of a cube array with $\lambda_p = 25\%$ are also included. The contribution of S2 ($u' < 0, w' > 0$) mode and S4 ($u' > 0, w' < 0$) mode become large rapidly above $z/H = 0.5$. In addition, S4 mode have a larger contribution than S2 mode within and a little above the canopy, however, the magnitude relationship of the influence of these two modes become reverse and the effect of S2 mode is slightly larger for momentum transfer above $z/H = 1.25$. This tendency is consisted with the vertical distribution of skewness shown in Fig. 5(f) and (g). The transition of the contribution ratio of S2 mode and S4 mode is also confirmed in a cube array (Kanda et al., 2004) and vegetation canopy (e.g., Finnigan et al., 2009), thus this tendency is considered to be universal regardless of shape of roughness elements.

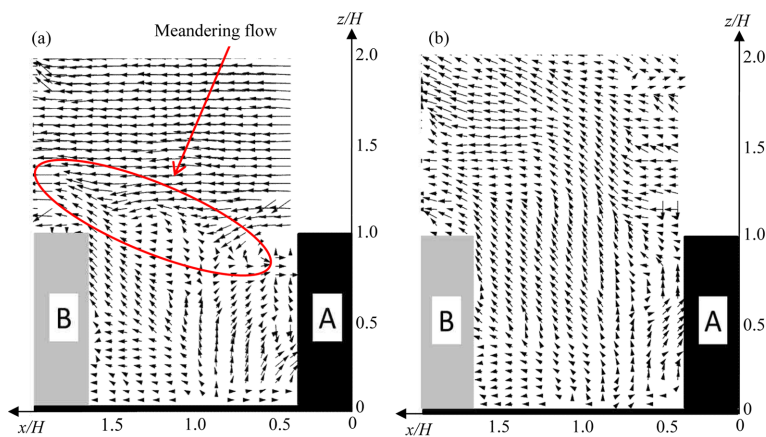


Figure 7(a)-(b). Vector maps of two characteristics flow patterns. Strong upward wind occur within the canopy in both instantaneous flow fields and the condition A is satisfied ($u' < 0, w' > 0$ are fulfilled more than 60% of measurement points in shaded square in Fig. 4).

As Fig. 5(b)-(g) shows, although standard deviation, Reynolds stress and uw correlation coefficient above the canopy height in the present experiment differ from those in vegetation canopy, all turbulent statistics presented here fall within the range of scattering of vegetation canopy under a height of $1.0H$. This result suggests that the flow characteristics characterized by the basic turbulent statistics in high-aspect-ratio block arrays is close to those in vegetation canopy under the canopy height.

4. Instantaneous Flow Field

4.1. Typical instantaneous upward flow fields

Several previous studies imply the possibility that some typical instantaneous flow patterns have a large contribution for momentum transfer between within and above canopy, for example, Takimoto (2011) performed a field measurement and a wind tunnel experiment using PIV and presented instantaneous wind vectors of strong upward flow happens almost entire the canopy layer and just above the canopy, and they call this flow pattern as “Flushing”. Similar type flow patterns were also observed in numerical study; Inagaki (2011) performed LES of airflow over a cubical array assuming atmospheric boundary layer (ABL) in daytime and demonstrated that temperature within the canopy become higher when a flushing event occurs and upward flow occupies whole of canopy. Under the circumstances, we investigated the features of instantaneous flow fields when the flow satisfies one of the following criteria, A) upward mode: $u' < 0$ and $w' > 0$ are fulfilled more than 60% of shaded square, B) downward mode: velocity of more than 60% of the area is $u' > 0$ and $w' < 0$, and extracted six typical flow patterns.

Figure 7(a) and (b) show vector maps of typical upward mode which satisfy the condition A. In Fig. 7(a), obliquely upward flow covers entire the canopy layer, in contrast, the flow over the canopy is relatively smooth and parallel to the roof and the boundary of these two flow results in

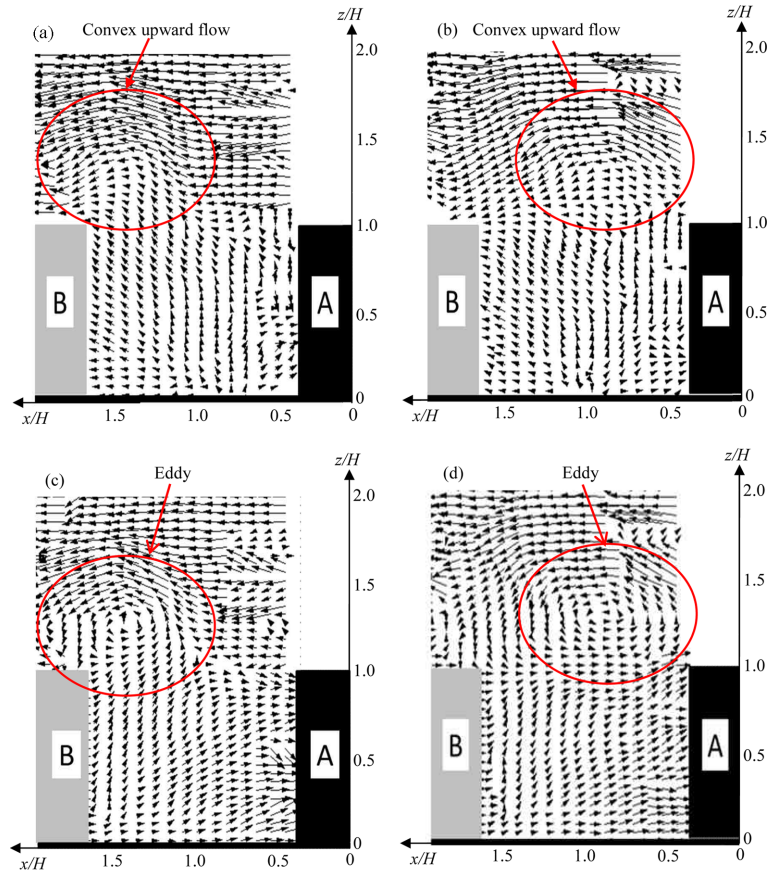


Figure 8. (a) and (b) Instantaneous flow fields captured at 26.780s and 26.760s after experiment began, both two satisfied condition A. (c) and (d) vector views produced by subtracting convective wind speed ($U_C = 0.25$) from Fig. 8(a) and (b) according to the method Adrian et al. (2000) developed.

meandering flow near the roof (red ellipse). Wind above the canopy is prevented from penetrating into the canopy by upward flow within the canopy and glides over canopy like skimming flow (Oke, 1988). In contrast, Fig. 7(b) illustrates not only within the canopy but also above the canopy up to a height of $2.2H$ are occupied by strong obliquely upward mode with about 45 degree angle. This type of flow pattern moves downward with time maintaining its intensity.

Fig. 8(a) and (b) present two instantaneous flow fields which also satisfy the condition A, and the one illustrated in Fig. 8(b) was captured 0.02 seconds (twenty frames) prior to Fig. 8(a). These two flow patterns depict intermediate behavior of the two flow patterns presented in Fig. 7, namely, strong obliquely upward flow within the canopy extends to outside of the canopy but the top of that flow remains at $z/H = 1.4$. Furthermore, parabolic flows are observed inside the red circles in both figures and streamwise flows from upper stream circumvent that hyperbolic streamline. These types of flow patterns are obviously similar to the flushing mode Takimoto et al. (2011) presented, furthermore, they suggested that the mean duration time and frequency of flushing mode are 2-5 seconds and once in 2-3 minutes, respectively.

Considering the fact that the block size of Takimoto et al. (2011) is 60 times of the present study and the effect of wind speed is negligible because the order of the wind speed is same in both experiments, the averaged continuous time and frequency of this flow pattern in present study, 0.103 seconds and once in 2.6 seconds, are approximately consistent with them.

Next, we try to extract vortices associated with coherent structures from Fig. 8(a) and (b) by using a method Adrian et al. (2006) used. Fig. 8(c) and (d) show the vector map of $(u - U_C, w)$ produced by subtracting convection velocity, $U_C = 0.25$, based on the data of Fig. 8(a) and (b). It is notable that the locations of two large eddies observed in Fig. 8(c) and (d) are correspond to the position of the convex upward flow in Fig. 8(a) and (b). All snapshots during 0.02 sec. show agreement of locations of the convex upward flow and these eddies. Another point to note is that the eddy in Fig. 8(c) has a large influence on the flow field within the canopy. Stream lines drawn by vectors suggest that the effect of the eddy reaches to a height of $z = 0.35H$ and air within the canopy is plucked up to outside the canopy. These vector maps illustrate a direct correlation between canopy flow and turbulent organized structure above the canopy.

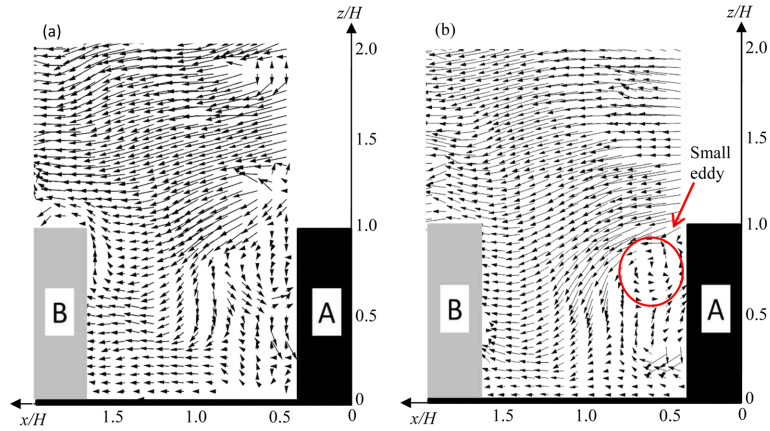


Figure 9. Vector maps of two characteristic flow patterns. Strong downward wind occurs above the canopy and it penetrates into canopy. The threshold B is satisfied in both flow field ($u' > 0$, $w' < 0$ are fulfilled more than 60% of measurement points in shaded square in Fig. 4).

4.2. Typical instantaneous downward flow fields

Fig.9 (a) and (b) show the two typical instantaneous flow fields which satisfy the condition B where strong downward wind dominates above the canopy in both case and it penetrates into the canopy. Although the flow fields above the canopy are almost same, the flow regimes within the canopy are significantly different.

In Fig. 9(a), the slantwise downward flow comes from

the upper layer separates into three parts. The one near the obstacle A changes its direction, resulting in a small wake vortex around a corner of block A. On the other hand, the one located at $x = 0.9H$ descends almost vertically and the other penetrates downward obliquely. In contrast, in Fig. 9(b), the strong downward flow from above the canopy is not separated into three parts and a small eddy is observed just behind the obstacle A, which stays in the

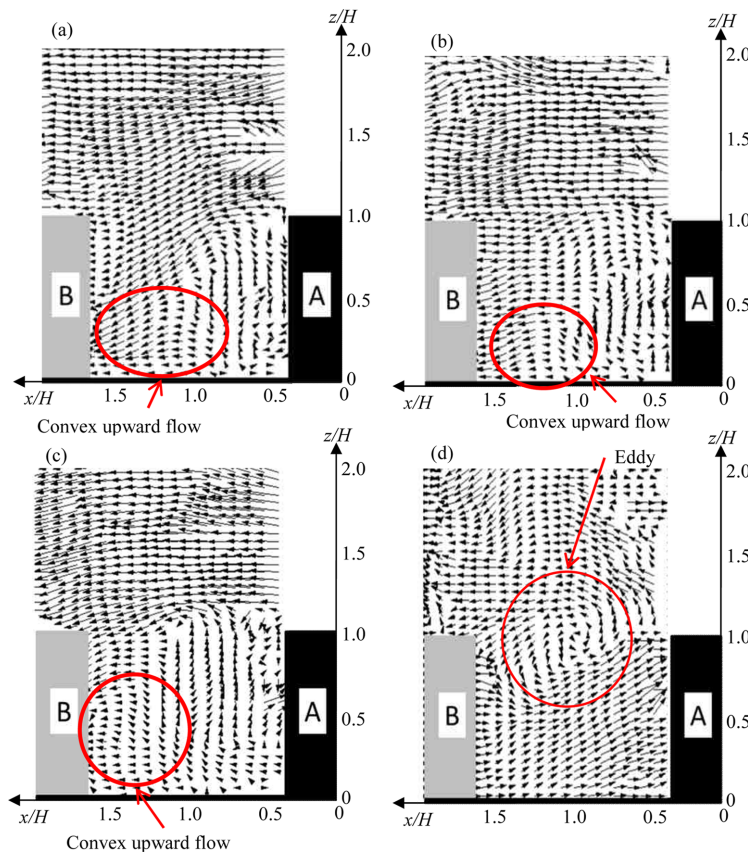


Figure 10. (a), (b) and (c) Instantaneous flow patterns at the moment when strong bent flow observed at the canopy roof height. (d) Vector views produced by subtracting convective wind speed ($U_C = 0.35$) from Fig. 10(a).

same position and gradually collapse with the decrease of intensity of the downward flow. This small eddy is supposed to be generated by the strong shear stress due to the strong downward flow come from above the canopy and low speed stream near the obstacle A.

Fig. 10(a), (b) and (c) show other typical instantaneous flow fields which fulfill the condition B. The most notable feature is the stream near the obstacle A: which bends sharply near the roof height. Specifically, small upward flow from the bottom of the canopy reaches to the canopy roof height and is affected by the strong downward flow from above the canopy, and finally incorporates into downward wind. In addition to this bent shape flow, small parabolic flows observed near the bottom of the canopy (red circles) in Fig. 10(a), (b) and (c). Although the size, intensity, and position of these small convex upward flows are not same, similar small hilly streams can be observed not only these three flow fields but also almost all of this type flow fields happen at different times.

Fig. 10(d) shows the large eddy at the canopy roof height advected by convection velocity, $U_C = 0.35$, in flow field Fig. 10(c) presented. Similar to Fig. 8, the location of the eddy completely corresponds to the position of the bent flow, and furthermore, the location of inverse flow which consists of a part of this eddy is in according with the gap between the bent flow and small hilly flow. Although the size of the eddy is little smaller than that shown in Fig. 8 (c) and (d), the eddy have a large influence on flow filed and determine the flow structure within the canopy.

5. Conclusions

In the present study, PIV measurement on the air flow around an urban-like canopy consists of blocks with high aspect ratio assuming an array of high-rise buildings revealed typical instantaneous flow patterns associated with turbulent organized structure (TOS) as follows.

First notable point is that the instantaneous flow filed for upward mode presented in Fig. 8(a) is quite similar to the typical instantaneous flow pattern called flushing (Takimoto et al., 2011; Inagaki et al., 2011) in both qualitative and quantitative aspects. Although transport phenomena of heat and pollutant materials are out of scope of this study, previous studies suggested that flushing mode appears around low-aspect building models has a large influence on the heat and pollutant removal (e.g., Michioka et al.), hence, it might be considered that the flow field presented in present study also strongly relates to the heat and air pollutant condition around high-rise buildings.

Second remarkable result is five typical instantaneous flow patterns which enhance the mixing of the air between canopy layer and roughness sub layer. Large scale downward flow presented in previous studies is also observed in present study, and moreover, it divided into three typical patterns based on flow field within the canopy. In particular, the flow filed when strong bent flow occur

(Fig. 10(a), (b) and (c)) were quite complicated, specifically, the air once uprises from the bottom of the canopy to the roof height and then descends into the canopy with strong downward wind from above the canopy. To understand the influence of this flow field on the scalar transfer, further investigation is needed, nevertheless it might be predicted that temperature and scalar concentration within a canopy is significantly related with such a specific flow field.

Adrian et al. (2006) presented a stream of a series of eddies as an indication of cross section surface of hairpin packet structure in surface layer over a smooth wall. Although it is not definitive that the eddies shown in the present study are parts of hairpin packet structure because only one eddy was observed in each vector views (Fig. 8 (c), (d) and Fig. 10(d)) due to the small measurement area, the condition of flow field around these eddies are well correspond to that they defined as the feature of the hairpin packet structure. It is interesting if the large eddy above the canopy associated with a hair-pin packet structure result in a certain type of instantaneous flow filed within the canopy. Future work will aim to acquire instantaneous flow field with wider measurement area to corroborate the present conjecture.

References

- Adrian, R. J., Meinhart, C. D. and Tomkins, C. D. (2000). "Vortex organization in the outer region of the turbulent-boundary layer." *Journal of Fluid Mechanics*, CUP, 422, pp. 1~54.
- Amiro, B. D. (1990). "Comparison of turbulence statistics within three boreal forest canopies." *Boundary-Layer Meteorology*, KAP, 51(1-2), pp. 99~121.
- Baldocchi, D. D. and Meyers, T. P. (1988). "Turbulence structure in a deciduous forest." *Boundary-Layer Meteorology*, KAP, 43(4), pp. 345~364.
- Coccal, O., Thomas, T. G., Castro, I. P. and Belcher, S. E. (2006). "Mean flow and turbulent statistics over groups of urban-like cubical obstacles." *Boundary-Layer Meteorology*, KAP, 121(3), pp. 491~519.
- Denmead, O. T. and Bradley, E. F. (1987). "On scalar transport in plant canopies." *Irrigation Science*, S.V., 8(2), pp. 131~149.
- Finnigan, J. J., Shaw, R. H. and Patton, E. G. (2009). "Turbulent structure above a vegetation canopy." *Journal of Fluid Mechanics*, CUP, 637, pp. 387~424.
- Grimmond, C. S. B. and Oke, T. R. (1998). "Aerodynamic properties of urban areas derived from analysis of surface form." *Journal of Applied Meteorology*, AMS, 38(9), pp. 1262~1292.
- Hagishima, A., Ikegaya, N., Tanimoto, J. and Yamaguchi, M. (2012). "Drag coefficients of staggered arrays with various block aspect ratio." Proc. 8th International Conference on Urban Climates (ICUC8), IAUC, Ireland.
- Huq, P., White, L. A., Carrillo, A., Redondo, J., Dharmavaram, S. and Hanna, S. R. (2007). "The shear layer above and in urban canopies." *Journal of Applied Meteorology*

- and *Climatology*, AMS, 46(3), pp. 368~376.
- Inagaki, A., Castillo, M. L., Yamashita, Y., Kanda, M. and Takimoto, H. (2011). "Large-eddy simulation of coherent flow structures within a cubical canopy." *Boundary-Layer Meteorology*, KAP, 142(2), pp. 207~222.
- Kanda, M., Moriwaki, R. and Kasamatsu, F. (2004). "Large-eddy simulation of turbulent organized structures within and above explicitly resolved cube arrays." *Boundary-Layer Meteorology*, KAP, 112(2), pp. 343~368.
- Kanda, M. (2006). "Large eddy simulations of the effects of surface geometry of building arrays on turbulent organized structure." *Boundary-Layer Meteorology*, KAP, 118(1), pp. 151~168.
- Li, X., Liu, C. and Leung, D. Y. C. (2008). "Large-eddy simulation of flow and pollutant dispersion in high-aspect-ratio urban street canyons with wall model." *Boundary-Layer Meteorology*, KAP, 129(2), pp. 249~268.
- Macdonald, R. W., Carter, S. S. and Slawson, P. R. (2002). "Physical modelling of urban roughness using arrays of regular roughness elements." *Water, Air and Soil Pollution: Focus*, KAP, 2(5-6), pp. 541~554.
- Michioka, T., Sato, A., Takimoto, H. and Kanda, M. (2011). "Large-eddy simulation for the mechanism of pollutant removal from a two-dimensional street canyon." *Boundary-Layer Meteorology*, KAP, 138(2), pp. 195~213.
- Moriwaki, R., Fujimori, Y. and Aoki, S. (2009). "Comparison of turbulence statistics above outdoor urban scale model and rice paddy." Proc. 7th International Conference on Urban Climate (ICUC-7), IAUC, Japan.
- Oke, T. R. (1988). "Street design and urban canopy layer climate." *Energy and Buildings*, EVB, 11(1-3), pp. 103~113.
- Pokrajac, D., Campbell, L., Nikora, V., Manes, C. and McEwan, L. (2007). "Quadrant analysis of persistent spatial velocity perturbations over square-bar roughness." *Experiments in Fluids*, Springer-Verlag, 42(3), pp. 413~423.
- Raupach, M. R., Finnigan, J. J. and Brunet, Y. (1996). "Coherent eddies and turbulence in vegetation canopies: The mixing-layer analogy." *Boundary-Layer Meteorology*, KAP, 78(3-4), pp. 351~382.
- Reynolds, R. and Castro, I. (2008). "Measurements in an urban-type boundary layer." *Experimental in Fluids*, Springer-Verlag, 45(1), pp. 141~156.
- Takimoto, H., Sato, A., Barlow, J. F., Moriwaki, R., Inagaki, A., Onomura, S. and Kanada, M. (2011). "Particle image velocimetry measurements of turbulent flow within outdoor and indoor urban scale models and flushing motions in urban canopy layers." *Boundary-Layer Meteorology*, KAP, 140(2), pp. 295~314.
- Westerweel, J. (1994). "Efficient detection of spurious vectors in particle image velocimetry data." *Experiments in Fluids*, Springer-Verlag, 16(3-4), pp. 236~247.
- Willert, C. E. and Gharib, M. (1990). "Digital particle image velocimetry." *Experiments in Fluids*, Springer-Verlag, 10(4), pp. 181~193.